Chinese Journal of Natural Medicines

New diterpenoids from *Euphorbia wallichii* with antioxidant activity

Yali Wang, Juan Chen, Wenshuo Zheng, Ziyan Gao, Yuxin Gan, Hua Li, Lixia Chen

Citation: Yali Wang, Juan Chen, Wenshuo Zheng, Ziyan Gao, Yuxin Gan, Hua Li, Lixia Chen, New diterpenoids from *Euphorbia wallichii* with antioxidant activity, Chinese Journal of Natural Medicines, 2025, 23(10), 1248−1258. doi: 10.1016/S1875−5364(25)60859−4.

View online: https://doi.org/10.1016/S1875−5364(25)60859−4

Chinese Journal of Natural Medicines 23 (2025) 1248-1258

Contents lists available at ScienceDirect

Chinese Journal of Natural Medicines

journal homepage: www.cjnmcpu.com/

Original article

New diterpenoids from *Euphorbia wallichii* with antioxidant activity

Yali Wang[a], Juan Chen[a], Wenshuo Zheng[a], Ziyan Gao[a], Yuxin Gan[b], Hua Li[a,*], Lixia Chen[b,*]

[a] *Institute of Structural Pharmacology & TCM Chemical Biology, Fujian Key Laboratory of Chinese Materia Medica, College of Pharmacy, Fujian University of Traditional Chinese Medicine, Fuzhou 350122, China*

[b] *Wuya College of Innovation, Key Laboratory of Structure-Based Drug Design & Discovery, Ministry of Education, Shenyang Pharmaceutical University, Shenyang 110016, China*

ARTICLE INFO

Article history:
Received 23 July 2024
Revised 11 October 2024
Accepted 16 October 2024
Available online 20 October 2025

Keywords:
Euphorbia wallichii
Tiglianes
Rhamnofolanes
Daphnanes
Antioxidant activity

ABSTRACT

Thirteen novel diterpenoids, comprising seven tiglianes (walliglianes G–M, **1**–**7**), four rhamnofolanes (wallinofolanes A–D, **8**–**11**), and two daphnanes (wallaphnanes A and B, **12** and **13**), together with two known rhamnofolane diterpenoids (euphorwallside H and euphorwallside I, **14** and **15**), were isolated and characterized from *Euphorbia wallichii* (*E. wallichii*). The chemical structures of these compounds were elucidated through nuclear magnetic resonance (NMR), mass spectrometry (MS), and quantum chemical calculations. Compounds **9** and **11** demonstrated protective effects against H_2O_2-induced BV-2 microglial cell damage. Molecular docking analyses indicated that compound **9** exhibited binding affinity to the antioxidant-related targets HMGCR, GSTP1, and SHBG.

1. Introduction

Tiglianes, rhamnofolanes, and daphnanes represent biogenetically related diterpenoids, primarily derived from plants of the *Euphorbia wallichii* (*E. wallichii*) Hook. f. (Euphorbiaceae) and Thymelaeaceae families [1]. These diterpenoids share a common 5/7/6 ring skeleton but exhibit differences in the C-ring appendage (C16-C15-C17), forming a cyclopropane moiety (C13-C14-C15) in tiglianes. In rhamnofolanes or daphnanes, the appendage constitutes an isopropyl group at C-14 or C-13. From a biosynthetic perspective, rhamnofolanes and daphnanes can originate from cyclopropane-ring opening of tiglianes [2]. Studies demonstrate that these compounds exhibit significant pharmacological effects, including anti-oxidant, anti-HIV, anti-tumor, and anti-α-glucosidase properties [3–6]. Given their structural diversity and notable pharmacological activities, natural products remain a vital source for drug discovery [7].

E. wallichii belongs to the genus *Euphorbia* of the family Euphorbiaceae, predominantly distributed in the Qinghai-Tibetan Plateau region of China, India, Nepal, and Kashmir [8]. Previous investigations have demonstrated that *E. wallichii* contains abundant diterpenoids, several of which demonstrate anti-oxidant, anti-inflammatory, anti-tumor, anti-microbial, and ion channel-blocking activities [6, 9–11]. Research has established that tigliane/rhamnofolanes glycosides from *E. wallichii* demonstrate effectiveness in preventing oxidative stress-induced neuronal death. Additionally, euphwanoid A isolated from *E. wallichii* exhibited significant anti-oxidant activity [6, 12]. These compelling findings motivated further investigation into potential anti-oxidant diterpenoids from *E. wallichii*. This study examines the whole plant of *E. wallichii* phytochemically. All isolated compounds were evaluated for anti-oxidant activities in the H_2O_2-induced BV-2 microglial cells damage model.

2. Results and discussion

The investigation yielded thirteen previously undescribed diterpenoids, comprising seven tiglianes (walliglianes G–M, **1**–**7**), four rhamnofolanes (wallinofolanes A–D, **8**–**11**), and two daphnanes (wallaphnanes A and B, **12** and **13**), alongside two known rhamnofolane diterpenoids (euphorwallside H and euphorwallside I, **14** and **15**) [6]. These compounds were isolated and characterized (Fig. 1).

Wallighane G (**1**) was isolated as a white powder and assigned the molecular formula $C_{20}H_{28}O_5$, with 7 degrees of unsaturation determined from high-resolution electrospray ionization mass spectrometry (HR-ESI-MS) (*m/z* 349.2002 $[M + H]^+$) and ^{13}C nuclear magnetic resonance (NMR) data. The ^{13}C NMR and heteronuclear single quantum correlation (HSQC) spectra of **1** (Tables 1 and 3) exhibited 20 carbon resonances comprising four methyl groups [δ_H 1.82 (3H, d, J = 1.2 Hz, H_3-19), 1.24 (3H, s, H_3-20), 1.21 (3H, s, H_3-17), and 0.95 (3H, d, J = 6.9 Hz, H_3-18); δ_C 24.9 (C-20), 15.5 (C-18), 11.0 (C-17), and 10.8 (C-19)], one trisubstituted double bond [δ_H 7.23 (1H, br s, H-1); δ_C 155.8 (C-1) and 141.3 (C-2)], one hydroxymethyl group [δ_H 3.75 (1H, d, J = 10.4 Hz, H-16a) and 2.97 (1H, d, J = 10.4 Hz, H-16b); δ_C 73.9 (C-16)], one oxygenated methine [δ_H 3.63 (1H, d, J = 7.2 Hz, H-7); δ_C

* Corresponding author.
E-mail addresses: lihua@fjtcm.edu.cn (H. Li); syzyclx@163.com (L. Chen)

https://doi.org/10.1016/S1875-5364(25)60859-4

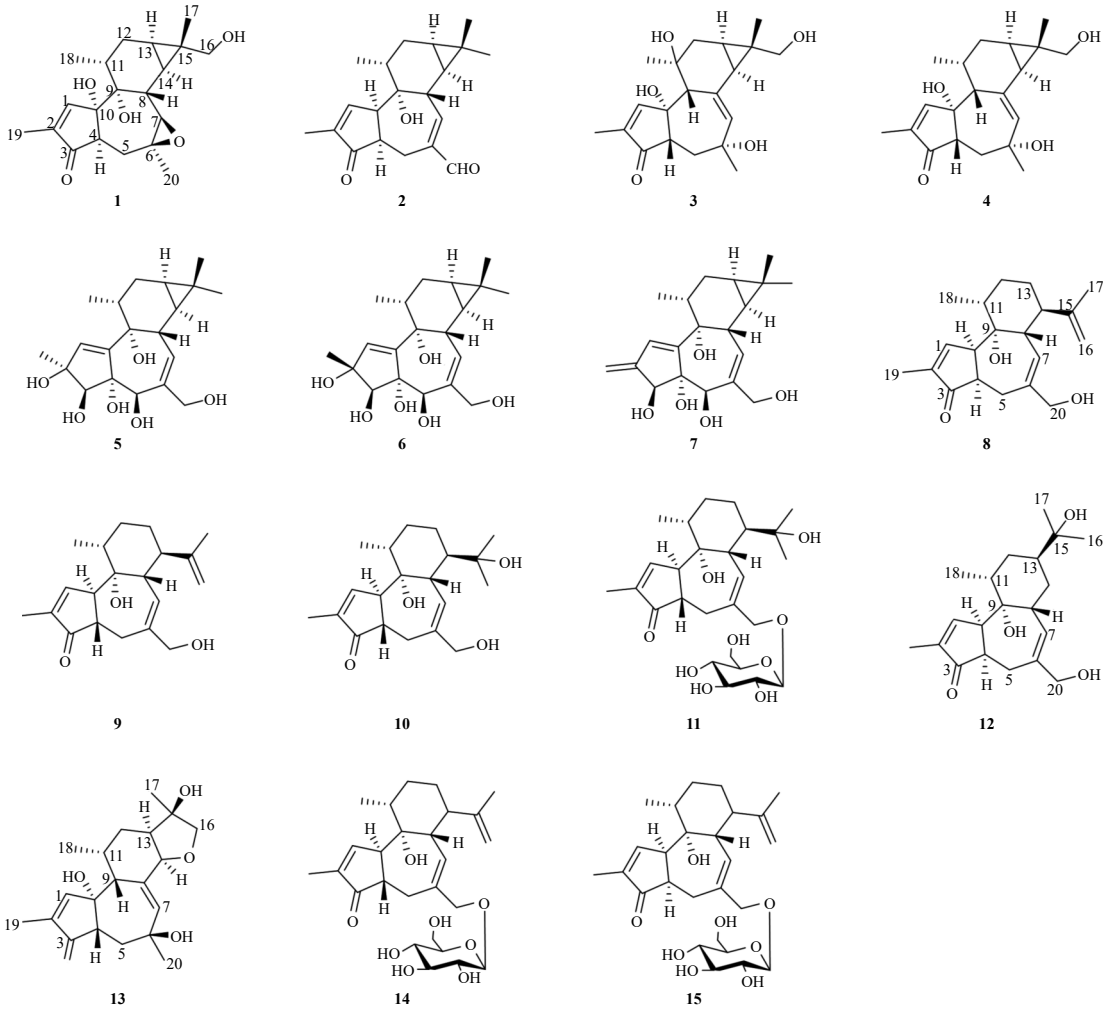

Fig. 1 Structures of **1**–**15** isolated from *E. wallichii*.

88.0 (C-7)], three oxygenated tertiary carbons [δ_C 83.4 (C-9), 82.8 (C-10), and 78.6 (C-6)], two cyclopropane methines [δ_H 0.79 (m, H-13) and 0.75 (m, H-14); δ_C 23.7 (C-14) and 16.0 (C-13)], and a ketocarbonyl δ_C 209.1 (C-3). These spectral characteristics indicated that **1** was a tigliane-type diterpenoid [13] potentially containing four hydroxyl groups. However, HR-ESI-MS data indicated 18 mass units less than the predicted structure, suggesting the presence of an epoxide group in compound **1**. The structure elucidation was supported by heteronuclear multiple bond correlation (HMBC). The HMBC of H_3-19 (δ_H 1.82) with C-1 (δ_C 155.8)/C-2 (δ_C 141.3)/C-3 (δ_C 209.1) and H-1 (δ_H 7.23) with C-3 (δ_C 209.1) confirmed that Δ^1 conjugated with the keto carbon (δ_C 209.1, C-3). The 6,7-epoxide group was established through HMBC of H_3-20 (δ_H 1.24) with C-5 (δ_C 28.7)/C-6 (δ_C 78.6)/C-7 (δ_C 88.0) and H-7 (δ_H 3.63) with C-5 (δ_C 28.7)/C-8 (δ_C 40.8)/C-14 (δ_C 23.7). The 16-CH_2OH was confirmed by HMBC correlations of H_2-16 (δ_H 3.75 and 2.97) with C-14 (δ_C 23.7)/C-15 (δ_C 27.3)/C-17 (δ_C 11.0). The OH at C-9 was established through HMBC from H-4 (δ_H 2.39) and H-8 (δ_H 2.10) to the oxygenated tertiary carbon (δ_C 83.4) (Fig. 2). Nuclear Overhauser effect spectroscopy (NOESY) spectrum analysis revealed cross-peaks of H-7 with H-13/H-14, H_3-20 with H-7/H-5b/H-14, and H-4 with H-5b, indicating α-orientation of these protons. Additionally, NOE correlations of H_3-17 with H-11 and H_2-16 with H-13/H-14 indicated β-orientation of H-11 (Fig. 3). ^{13}C NMR calculations for **1**-4*R** and **1**-4*S** were performed, and DP4+ probability analysis (Fig. 4) suggested 4*R** as the correct configuration for wallichiane G (**1**). The absolute configuration of **1** was determined by comparing computational and experimental electronic circular dichroism (ECD). As shown in Fig. 5, the experimental ECD spectrum of **1** displayed Cotton effects at 318 (+), 232 (−), and 205 (+) nm, corresponding to the calculated spectrum (4*R*,6*S*,7*R*,8*R*,9*R*,10*S*,11*R*,13*R*,14*R*,15*S*)-**1**, confirming identical absolute configuration. The structure of compound **1**, wallichiane G, was thus established as shown.

Wallichiane H (**2**) was isolated as a white amorphous powder with a molecular formula of $C_{20}H_{26}O_3$, determined through HR-ESI-MS (*m/z* 337.1768 $[M + Na]^+$, Calcd. for $C_{20}H_{26}O_3Na$, 337.1780) and NMR data. The ^{1}H and ^{13}C NMR data of **2** revealed four methyl groups [δ_H 1.74 (3H, s, H_3-19), 1.08 (3H, s, H_3-16), 1.04 (3H, s, H_3-17), and 1.02 (3H, d, J = 6.5 Hz, H_3-18); δ_C 29.2 (C-16), 16.5 (C-17), 15.5 (C-18), and 10.7 (C-19)], two trisubstituted double bonds [δ_H 7.03 (1H, s, H-1) and 6.18 (1H, t, J = 3.2 Hz, H-7); δ_C 155.7 (C-1), 154.9 (C-7), 143.7 (C-2), and 139.2 (C-6)], a formyl group [δ_H 9.32 (1H, s), δ_C 194.6], one oxygenated tertiary carbons δ_C 75.8 (C-9), and a ketocarbonyl δ_C 210.7 (C-3). Analysis of the NMR data, along with examination of 2D NMR data, indicated that the structure of **2** exhibited close similarity to 20-formyl-4 α-deoxyphorbol-13-acetate, differing in the absence of the hydroxy group at C-12 and the acetoxy group at C-13 in **2** [14]. This structural difference was confirmed by the chemical shifts of C-12 (δ_C 25.4) and C-13 (δ_C 19.7), supported by HMBC from H_3-18 (δ_H 1.02) to C-9 (δ_C 75.8)/C-11 (δ_C 36.5)/C-12 (δ_C 25.4) and H-12a (δ_H 1.81)/H_3-16 (δ_H 1.08)/H_3-17 (δ_H 1.04) to C-13 (δ_C 25.4) (Fig. 2). The relative configuration of **2** was determined to be identical that of 20-formyl-4α-deoxyphorbol-13-acetate through comparison of their NOESY data [14]. The NOESY spectrum exhibited key correlations of H-10 with H-4/H_3-18, confirming α-orientation for H-4 and 18-CH_3. Furthermore, ^{13}C NMR calculations

Table 1 ^{1}H NMR (600 MHz) data for compounds **1**–**7**.

No.	**1**[a]	**2**[a]	**3**[a]	**4**[a]	**5**[b]	**6**[b]	**7**[a]
1	7.23, br s	7.03, s	7.77, br s	7.22, br s	5.68, br s	5.69, s	6.30, s
3					3.67, s	3.70, s	4.33, s
4	2.39, dd (8.4, 5.0)	2.84, m	2.68, dd (9.5, 7.6)	2.68, dd (9.7, 7.2)			
5	2.37, dd (13.9, 8.4) 1.58, dd (13.9, 5.0)	3.28, dd (15.7, 4.5) 3.02, m	2.32, dd (11.7, 9.5) 1.61, dd (11.7, 7.6)	2.32, dd (11.7, 9.7) 1.67, m	4.27, s	4.03, s	3.77, s
6							
7	3.63, d (7.2)	6.18, t (3.2)	5.94, d (2.0)	5.94, d (2.0)	5.72, d (6.0)	5.66, d (5.7)	5.72, d (4.6)
8	2.10, dd (7.2, 3.1)	2.02, m		1.94, m	3.15, t (5.7)	3.14, t (5.3)	3.12, t (4.6)
9			1.96, br s				
10		3.54, m					
11	2.20, m	1.52, m		2.07, m	1.37, m	1.39, m	1.40, m
12	1.77, m 1.51, m	1.81, m 1.66, m	2.07, dd (14.2, 10.1) 1.58, dd (14.2, 3.9)	1.90, m 1.67, m	1.66, dd (14.6, 7.3) 1.57, m	1.67, dd (14.6, 7.3) 1.58, m	1.77, dd (15.0, 7.1) 1.55, m
13	0.79, m	0.82, t (8.5)	1.19, m	1.10, m	0.72, m	0.72, m	0.79, m
14	0.75, m	0.41, dd (9.1, 6.4)	1.45, d (9.1)	1.44, d (9.1)	0.57, dd (9.4, 5.5)	0.55, dd (9.5, 5.2)	0.58, dd (9.1, 5.4)
16	3.75, d (10.4) 2.97, d (10.4)	1.08, s	3.34, d (10.8) 3.32, d (10.8)	3.33, d (10.9) 3.31, d (10.9)	1.05, s	1.05, s	1.09, s
17	1.21, s	1.04, s	1.21, s	1.17, s	0.98, s	0.99, s	1.01, s
18	0.95, d (6.9)	1.02, d (6.5)	1.40, s	1.04, s	0.74, s	0.81, d (6.7)	0.80, d (6.6)
19	1.82, d (1.2)	1.74, s	1.78, d (1.3)	1.81, d (1.4)	1.33, s	1.39, s	5.22, s 5.14, s
20	1.24, s	9.32, s	1.37, s	1.36, s	4.10, d (12.6) 4.04, d (12.6)	4.12, d (11.9) 3.96, d (11.9)	4.23, d (11.8) 4.16, d (11.8)

[a] Recorded in $CDCl_3$; [b] Recorded in methanol-d_4.

for **2**-4*R** and **2**-4*S** were performed, and DP4+ probability analysis (Fig. S4) indicated 4*R** as the correct configuration for walligliane H (**2**). The NOESY correlation of H-11 with H-8 established *β*-orientation for H-11 and H-8 (Fig. 3). The absolute configuration of **2** was established as 4*R*, 8*S*, 9*R*, 10*R*, 11*R*, 13*R*, 14*R* through comparison of computational and experimental ECD (Fig. S3). Thus, the structure of compound **2**, walligliane H, was characterized as shown.

Walligliane I (**3**) exhibited the molecular formula $C_{20}H_{28}O_5$ determined by HR-ESI-MS ([M + HCOOH − H]$^-$ *m/z* 393.1889, Calcd. 393.1913). Analysis of 1D and 2D NMR spectra of **3** identified it as a tetracyclic tigliane-type diterpenoid [13]. The HMBC spectrum of **3** (Fig. 2) displayed key correlations from H_3-18 (δ_H 1.40) to C-11 (δ_C 75.4)/C-9 (δ_C 55.1)/C-12 (δ_C 39.2) along with the chemical shifts of C-11 (δ_C 75.4), indicating hydroxy and methyl moieties at C-11. The hydroxy group position at C-6 was confirmed by HMBC (Fig. 2) from H_3-20 (δ_H 1.37) to C-7 (δ_C 134.3)/C-6 (δ_C 84.4)/C-5 (δ_C 42.8), supported by the chemical shifts of C-6 (δ_C 84.4). The HMBC from both H_2-16 (δ_H 3.34 and 3.32) and H_3-17 (δ_H 1.21) to C-15 (δ_C 28.7)/ C-14 (δ_C 26.2)/ C-13 (δ_C 19.6) established a hydroxymethyl and a methyl group at C-15. Furthermore, the key HMBC of H-7 (δ_H 5.94) to C-14 (δ_C 26.2), H-9 (δ_H 1.96) to C-8 (δ_C 135.0), and H-5a (δ_H 2.32) to C-6 (δ_C 84.4)/ C-7 (δ_C 134.3) confirmed the location of $\Delta^{7(8)}$ double bond. The NOESY spectrum (Fig. 3), showed correlations of H_3-17 with H-9, H_2-16 with H-13, H_3-18 with H-12a, and H-12a with H-13, while lacking correlations of H_3-17/H-9 with H_3-18, demonstrating *α*-orientations of 18-CH_3 and 16-CH_2OH and *β*-orientation of H-9. The key NOESY correlations of H-4 with H-5a/H-9 and H_3-20 with H-5a indicated spatial proximity and *β*-orientation. Given the rarity of tiglianes with H-9 *β*-orientation in nature, quantum chemical calculations further validated this configuration. ^{13}C NMR calculations for **3** (9*S**) and **3-2** (9*R**) were performed, and DP4+ probability analysis (Fig. 6) indicated 9*S** as the correct configuration for walligliane I (**3**). The stereochemistry of **3** was determined as 4*S*, 6*R*, 9*S*, 10*R*, 11*S*, 13*R*, 14*R*, 15*S* based on ECD data (Fig. 5). Thus, the structure of compound **3** was established as shown.

Walligliane J (**4**) exhibited the molecular formula $C_{20}H_{28}O_4$, which is 16 mass units less than that of **3**, as determined by HR-ESI-MS ([M − H]$^-$ *m/z* 331.1920, Calcd. 331.1909). Analysis of NMR spectra revealed that the carbocyclic skeleton of **4** was identical to that of **3**, with the primary difference being the absence of the hydroxy group at C-11 in **4**. This structural determination was supported by the observation of HMBC of H_3-18 (δ_H 1.04) with C-9 (δ_C 49.0)/C-11 (δ_C 30.7)/C-12 (δ_C 28.0), along with the chemical shifts of C-11 (δ_C 30.7) (Fig. 2). The stereochemical configuration of **4** was determined to be identical to that of **3** through comparison of their NOE and ECD data (Fig. 3 and Fig. S3). The structure of compound **4**, walligliane J, was thus established as depicted.

Compound **5**, walligliane K, exhibited a molecular formula of $C_{20}H_{30}O_6$, determined through its HR-ESI-MS ion at *m/z* 365.1968 ([M − H]$^-$, Calcd. 365.1964, $C_{20}H_{29}O_6$) and ^{13}C NMR data. Analysis of the ^{13}C NMR and HSQC data for compound 5 identified 20 car-

Table 2 ^{1}H NMR (600 MHz) data for compounds **8**–**13**.

No.	**8**[a]	**9**[a]	**10**[a]	**11**[b]	**12**[a]	**13**[a]
1	7.21, br s	7.49, br s	7.45, br s	7.58, br s	7.14, br s	7.24, br s
4	2.74, m	2.62, td (9.7, 4.5)	2.48, m	2.65, m	2.72, m	2.79, dd (9.7, 7.1)
5	3.04, dd (16.3, 3.0) 2.64, dd (16.3, 4.7)	2.80, dd (17.6, 9.4) 2.16, dd (17.6, 10.0)	2.63, dd (15.9, 11.6) 1.96, dd (17.2, 7.9)	2.71, m 2.30, dd (16.9, 7.9)	2.88, dd (16.1, 2.6) 2.70, m	2.37, dd (11.9, 9.7) 1.69, dd (11.9, 7.1)
7	5.19, br s	5.35, d (6.7)	6.07, br d (6.1)	6.17, dd (7.5, 2.0)	5.11, br s	6.06, d (1.6)
8	1.92, d (12.0)	2.28, dd (11.3, 6.7)	2.12, dd (10.8, 8.0)	2.23, dd (11.0, 7.9)	2.44, br s	
9						2.42, m
10	3.55, m	3.09, m	3.08, m	3.24, m	3.46, m	
11	1.77, m	1.62, m	1.54, m	1.62, m	2.03, m	2.30, m
12	1.56, m 1.49, m	1.62, m 1.55, m	1.58, m 1.49, m	1.62, m 1.46, m	1.53, m 1.48, m	1.57, m 1.40, td (13.1, 4.0)
13	1.58, m 1.38, m	1.61, m 1.40, m	1.76, m 0.94, m	1.83, m 1.08, m	1.60, m	2.05, m
14	2.09, td (12.9, 3.3)	2.43, td (11.3, 3.3)	1.89, td (11.7, 3.2)	1.91, td (16.7, 3.6)	1.59, m 1.54, m	4.59, d (3.8)
16	4.76, br s 4.70, br s	4.76, br s 4.74, br s	1.18, s	1.17, s	1.21, s	3.89, d (9.5) 3.75, d (9.5)
17	1.59, s	1.57, s	1.04, s	1.14, s	1.20, s	1.32, s
18	1.13, d (6.7)	0.96, d (5.0)	0.91, d (6.2)	0.93, d (5.8)	1.10, d (6.7)	1.03, d (7.1)
19	1.80, d (1.2)	1.76, d (1.2)	1.72, d (1.0)	1.70, d (1.1)	1.79, d (1.1)	1.82, d (1.4)
20	3.95, d (12.1) 3.86, d (12.1)	3.99, d (12.9) 3.94, d (12.9)	3.98, d (15.9) 3.91, d (15.9)	4.18, d (12.0) 4.12, d (12.0)	4.01, d (12.5) 3.97, d (12.5)	1.37, s
1′				4.29, d (7.9)		
2′				3.14, t (8.2)		
3′				3.32, m		
4′				3.24, m		
5′				3.24, m		
6′				3.85, dd (12.0, 1.4) 3.61, dd (12.0, 5.2)		

[a] Recorded in $CDCl_3$; [b] Recorded in methanol-d_4.

bon resonances. These comprised four methyl groups [δ_H 1.33 (3H, s, CH_3-19), 1.05 (3H, s, CH_3-16), 0.98 (3H, s, CH_3-17), and 0.74 (3H, d, J = 6.6 Hz, CH_3-18); δ_C 29.4 (C-16), 24.1 (C-19), 18.1 (C-18), and 15.9 (C-17)], two trisubstituted double bonds [δ_H 5.72 (1H, d, J = 6.0 Hz, H-7) and 5.68 (1H, br s, H-1); δ_C 150.9 (C-10), 137.9 (C-1), 141.3 (C-6) and 136.1 (C-7)], one oxygenated methylene [δ_H 4.10 (1H, d, J = 12.6 Hz, H-20a) and 4.04 (1H, d, J = 12.6 Hz, H-20b); δ_C 67.4 (C-20)], two oxygenated methines [δ_H 4.27 (1H, s, H-5) and 3.67 (1H, s, H-3); δ_C 84.0 (C-3) and 73.8 (C-5)], and two oxygenated tertiary carbons [δ_C 83.9 (C-4) and 81.4 (C-2)]. The NMR data analysis indicated **5** was a tigliane-type diterpenoid [13]. The HMBC spectrum of **5** (Fig. 2) demonstrated key correlations from H_3-19 (δ_H 1.33) to C-1 (δ_C 137.9)/C-3 (δ_C 84.0)/C-2 (δ_C 81.4), H-3 (δ_H 3.67) to C-10 (δ_C 150.9)/C-1 (δ_C 137.9)/C-2 (δ_C 81.4)/C-5 (δ_C 73.8) and H-1 (δ_H 5.68) to C-10 (δ_C 150.9)/C-3 (δ_C 77.3), indicating hydroxy and methyl moieties at C-2, the hydroxy group at C-3, and the location of $\Delta^{1(10)}$ double bond. Further HMBC from H_2-20 (δ_H 4.10 and 4.04) to C-6 (δ_C 141.3)/C-7 (δ_C 136.1)/C-5 (δ_C 73.8) and H-5 (δ_H 4.27) to C-6 (δ_C 141.3)/C-7 (δ_C 136.1)/C-4 (δ_C 83.9) confirmed the presence of hydroxy group at C-4, C-5, and C-20. These findings established the gross structure of **5** as depicted. The NOESY correlations (Fig. 3, **5**) of H-8 with H-11/H_3-17 established these protons as β-oriented. Additionally, 19-CH_3 and H-3 were determined to be α-oriented, based on the correlations between H_3-19 and H-3/H_3-18. The NOESY correlations (DMSO-d_6) of 4-OH with H_3-19/9-OH and 5-OH with H-8 confirmed the α-orientation of 4-OH and 9-OH and β-orientations of 5-OH (Fig. 3, **5**[a]). Considering biosynthetic aspects of the β-orientation for 8-H and comparing computational and experimental ECD (Figure S3), the structure of **5** was determined as (2*S*, 3*S*, 4*R*, 5*R*, 8*S*, 9*R*, 11*R*, 13*R*, 14*R*) and named walligliane K [6,13].

Walligliane L (**6**) exhibited the same molecular formula of $C_{20}H_{30}O_6$ as **5** based on its HR-ESI-MS at m/z 365.1968 [M − H]$^-$.

Table 3 ^{13}C NMR (150 MHz) data for compounds **1**–**13**.

No.	**1**[a]	**2**[a]	**3**[a]	**4**[a]	**5**[b]	**6**[b]	**7**[a]	**8**[a]	**9**[a]	**10**[a]	**11**[b]	**12**[a]	**13**[a]
1	155.8	155.7	156.0	151.7	137.9	138.8	132.9	157.4	159.0	159.5	162.1	157.0	151.1
2	141.3	143.7	141.5	145.2	81.4	78.7	152.8	142.9	137.0	135.9	136.8	142.3	145.4
3	209.1	210.7	208.8	209.5	84.0	83.0	77.2	212.8	210.2	210.6	213.4	211.7	209.1
4	53.7	49.1	58.6	58.8	83.9	83.6	83.2	49.9	44.4	44.9	46.3	49.4	57.9
5	28.7	20.9	42.8	43.0	73.8	72.6	73.3	25.8	29.4	27.2	28.8	26.8	43.0
6	78.6	139.2	84.4	84.8	141.3	140.9	138.2	137.6	141.7	139.7	137.4	139.1	84.5
7	88.0	154.9	134.3	133.5	136.1	137.2	135.9	126.0	125.1	123.5	132.8	128.7	135.9
8	40.8	42.7	135.0	132.9	37.5	37.0	36.3	46.1	48.4	50.5	51.6	38.3	133.3
9	83.4	75.8	55.1	49.0	77.3	77.5	77.2	78.0	77.4	77.2	78.3	77.6	45.0
10	82.8	47.0	87.9	87.6	150.9	149.4	149.9	49.3	56.4	55.3	56.7	50.7	88.1
11	31.8	36.5	75.4	30.7	38.0	38.0	37.0	40.0	36.5	35.9	37.1	35.0	30.5
12	24.0	25.4	39.2	28.0	26.3	26.3	25.0	29.8	31.9	31.7	32.8	30.2	32.5
13	16.0	19.7	19.6	18.4	21.4	21.3	19.5	32.5	32.0	29.5	29.8	40.7	47.8
14	23.7	24.5	26.2	26.3	26.4	26.9	25.2	48.3	45.0	45.6	46.7	30.3	81.1
15	27.3	18.5	28.7	28.9	18.9	18.8	18.3	148.1	147.7	74.4	74.7	73.8	82.2
16	73.9	29.2	73.1	73.8	29.4	29.5	29.0	112.8	112.5	31.8	30.5	29.2	78.9
17	11.0	16.5	11.5	11.4	15.9	15.9	15.4	19.1	18.9	23.0	25.7	28.0	20.9
18	15.5	15.5	24.1	15.7	18.1	18.3	17.8	16.0	18.7	18.8	19.3	15.6	14.9
19	10.8	10.7	10.8	11.0	24.1	26.8	110.1	10.6	10.5	10.5	10.4	10.7	11.0
20	24.9	194.6	23.9	24.3	67.4	67.4	69.8	70.2	67.7	65.8	76.1	69.2	23.7
1′											103.6		
2′											75.2		
3′											78.0		
4′											71.8		
5′											78.2		
6′											62.9		

[a] Recorded in $CDCl_3$; [b] Recorded in methanol-d_4.

The comparable 1D NMR data (Tables 1 and 3) indicated that **6** shared an identical planar structure with **5**, which was verified by the HMBC (Fig. 2). In the NOESY spectrum (Fig. 3), the key correlations of H-8 with H_3-19 and absence of correlation between H_3-19 and H-3 demonstrated that 19-CH_3 was *β*-oriented, indicating that **5** and **6** were a pair of C-2 epimers. The absolute configuration of **6** was established as 2*R*, 3*S*, 4*R*, 5*R*, 8*S*, 9*R*, 11*R*, 13*R*, 14*R* through comparison of computational and experimental ECD (Fig. S3). Thus, the structure of compound **6** was determined as shown.

Walligliane M (**7**) displayed a molecular formula $C_{20}H_{28}O_5$, 18 mass units less than that of **5**, by HR-ESI-MS ($[M - H]^-$ *m/z* 347.1872, Calcd. 347.1858). NMR data of **7** resembled those of **5** except for C-1 ($\Delta\delta$ = −5.0), C-2 ($\Delta\delta$ = +71.4), C-3 ($\Delta\delta$ = −6.8), and C-19 ($\Delta\delta$ = +86.0), suggesting the presence of $\Delta^{2(19)}$ double bond in **7**, further confirmed by the HMBC of H_2-19 (δ_H 5.22 and 5.14) to C-2 (δ_C 152.8)/C-1 (δ_C 132.9)/C-3 (δ_C 77.2) (Fig. 2). The NOESY spectrum (Fig. 3) correlations of H_3-17 with H-8/H-11 and H-3 with H-5 indicated that the configurations of **7** matched those of **5**. The NMR chemical shifts for **7a** (9*R**) and **7b** (9*S**) were calculated at the mPW1PW91/6-31G(d,p) level. DP4+ probability analysis (Fig. S5) suggested **7a** as the correct structure for **7**. Consequently, the structure of compound **7** was established as shown.

Wallinofolane A (**8**) possesses a molecular formula of $C_{20}H_{28}O_3$ determined by the ion peak at *m/z* 523.3406 [M + HCOOH − H]$^-$ (calcd. for $C_{21}H_{29}O_5$, 361.2015) in HR-ESI-MS spectrum. The 1D NMR data confirmed that **8** represented the aglycone moiety of euphorwallside I [6]. This was further substantiated by HR-ESI-MS data and comprehensive 2D NMR analysis. The stereochemistry of **8** was determined to be identical to that of euphorwallside I through comparison of their NOESY and ECD data (Fig. 3 and Fig. S3). The structure of compound **8**, wallinofolane A, was therefore established as shown.

Wallinofolane B (**9**) exhibited the same molecular formula of $C_{20}H_{28}O_3$ as **8**, as evidenced by its HR-ESI-MS at *m/z* 361.1995 [M + HCOOH − H]$^-$, indicating its isomeric relationship with **8**. Analysis of the NMR data revealed that **9** represented the aglycone moiety of euphorwallside H [6]. The NOESY spectrum (Fig. 3) displayed key correlations of H-4 with H-8, demonstrating that H-4 adopted *β*-orientation in **9**. The experimental ECD of **9** aligned with computational ECD calculations, confirming its absolute configuration as 4*R*, 8*S*, 9*R*, 10*R*, 11*R*, 14*R* (Fig. S3). The structure was subsequently designated as wallinofolane B.

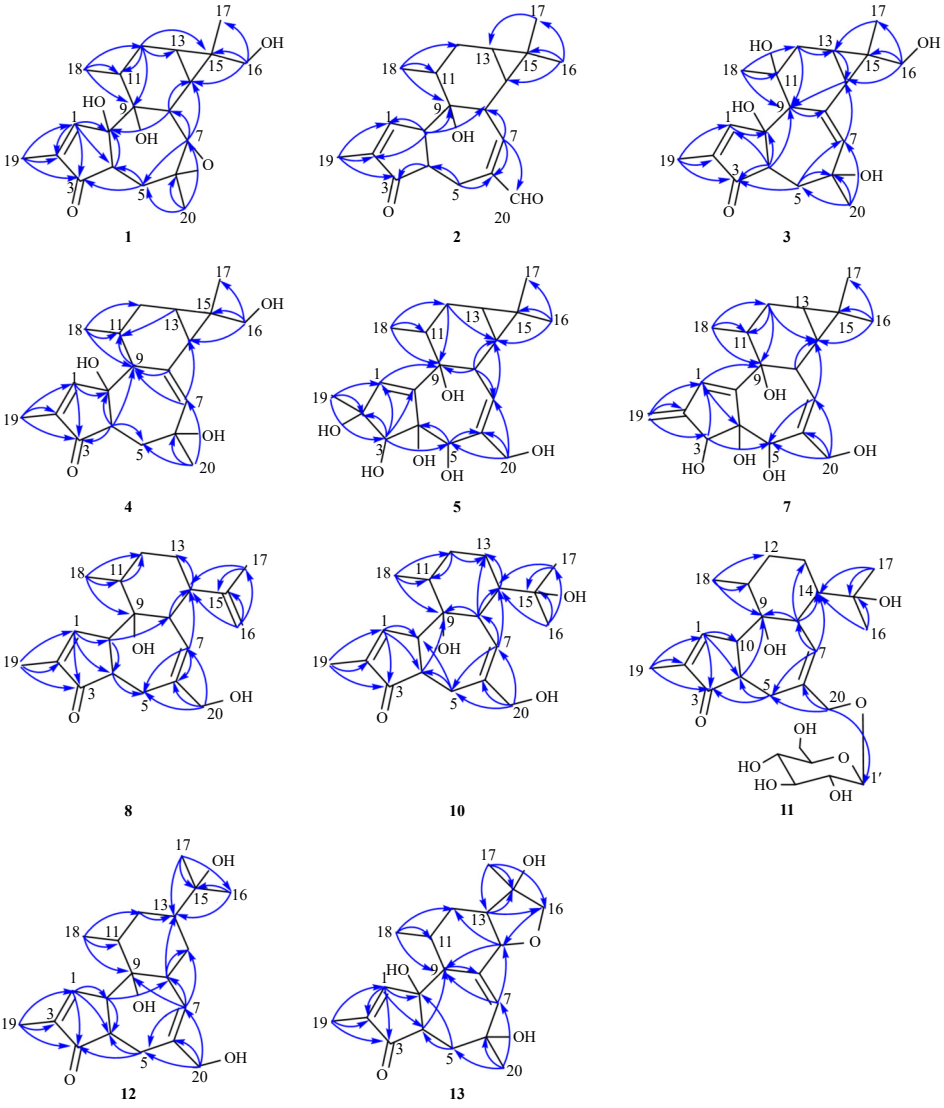

Fig. 2 HMBC correlations of compounds **1**–**5**, **7**, **8** and **10**–**13**.

Wallinofolane C (**10**) presented a molecular formula of $C_{20}H_{30}O_4$, determined by HR-ESI-MS ion at *m/z* 379.2143 [M + HCOOH – H]$^-$ (Calcd. for 379.2121), exceeding that of **9** by 18 mass units. Comparative analysis of NMR data between **10** and **9** indicated that the C-17 signal in **10** exhibited a deshielding effect of $\Delta\delta_C$ + 4.1 ppm, while C-15 and C-16 signals shifted by $\Delta\delta_C$ −73.3 and −80.7 ppm, respectively. Other carbon resonances showed shifts of $\Delta\delta_C \leq \pm$ 2.5 ppm. These observations suggested the replacement of Δ^{15} in **9** with a hydroxy group at C-15 in 10. This structural assignment was supported by detailed HMBC analysis, particularly the key correlations from H_3-16 (δ_H 1.18) to C-15 (δ_C 74.4)/C-14 (δ_C 45.6)/C-17 (δ_C 23.0) and from H_3-17 (δ_H 1.04) to C-15 (δ_C 74.4)/C-14 (δ_C 45.6)/C-16 (δ_C 31.8) (Fig. 2). The absolute configuration of **10** was determined to be identical to that of **9** (Fig. S3). The compound **10** was designated as wallinofolane C.

Wallinofolane D (**11**) exhibited a molecular formula of $C_{26}H_{40}O_9$, determined by its HR-ESI-MS ion at *m/z* 541.2660 ([M + HCOOH – H]$^-$, Calcd. 541.2649, $C_{27}H_{41}O_{11}$) and ^{13}C NMR data. The NMR spectra of **11** displayed similarities to compound **10**, with the notable addition of a *β*-glucose moiety in **11** [δ_H 4.29 (1H, d, *J* =7.9 Hz, H-1′), 3.85 (1H, dd, *J* =12.0, 1.4 Hz, H-6′a), 3.61 (1H, dd, *J* =12.0, 5.2 Hz, H-6′b), 3.32 (1H, m, H-3′), 3.24 (1H, m, H-4′), 3.24 (1H, m, H-5′), and 3.14 (1H, t, J =8.2 Hz, H-2′); δ_C 103.6 (C-1′), 78.2 (C-5′), 78.0 (C-3′), 75.2 (C-2′), 71.8 (C-4′), and 62.9 (C-6′)]. The position of the *β*-glucose group at C-20 was established through the HMBC of H_2-20 (δ_H 4.18 and 4.12) with C-1′ (δ_C 103.6) (Fig. 2). Furthermore, acid hydrolysis and appropriate derivatization of **11** confirmed the D-configuration of the glucosyl moiety (Fig. S8). Thus, the structure of **11** was established as depicted.

Wallaphnane A (**12**) shared the molecular formula with **10**, suggesting its nature as a positional isomer of **10**. Comprehensive HMBC analysis confirmed the gross structure of **12**, particularly through correlations from H_3-16 (δ_H 1.21) to C-15 (δ_C 73.8)/C-13 (δ_C 40.7)/C-17 (δ_C 28.0), from H_3-17 (δ_H 1.20) to C-15 (δ_C 73.8)/C-13 (δ_C 40.7)/C-16 (δ_C 29.2), and from H-7 (δ_H 5.11) to C-14 (δ_C 30.3) (Fig. 2). NOESY correlations (Fig. 3) between H-4 and H-10/H_3-18 indicated their *α*-orientation. The *α*-orientation of H-13 was determined based on correlations between H-8 and H_3-16/H_3-17. Analysis of calculated ^{13}C NMR chemical shifts for (9*R**)-**12** (**12a**) and (9*S**)-**12** (**12b**) revealed a DP4+ score of 100% for **12a** and 0% for **12b**, confirming the 9*R** configuration (Fig. S6). Comparison of computational and experimental ECD established the absolute configuration as 4*R*, 8*R*, 9*R*, 10*R* 11*R*, 13*R* by comparing the computational and experimental ECD (Fig. S3). Consequently, the structure of wallaphnane A (**12**) was established as illustrated.

Wallaphnane B (**13**) exhibited a molecular formula of $C_{20}H_{30}O_4$, determined from the HR-ESI-MS spectrum ([M – H]$^-$

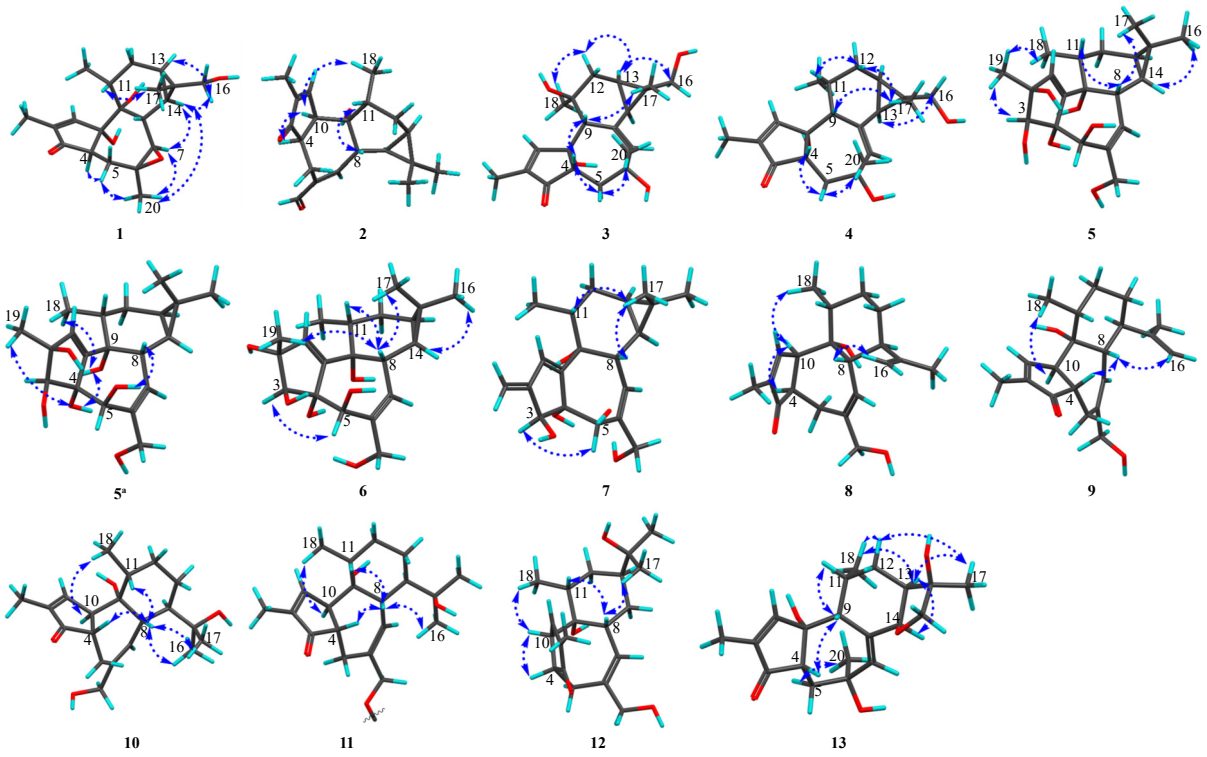

Fig. 3 NOESY correlations of compounds **1**–**13**.

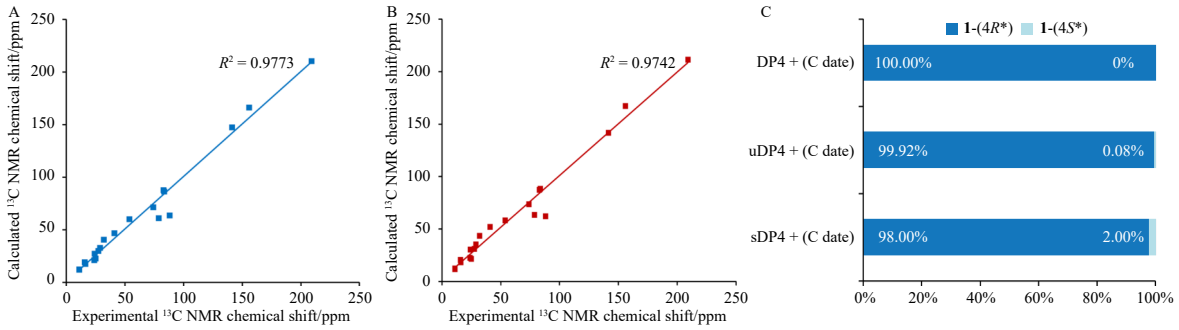

Fig. 4 Linear correlation between the experimental ^{13}C NMR data for **1** and the calculated data for **1**-4*R** (A) and **1**-4*S** (B), respectively. (C) DP4+ analysis between the ^{13}C NMR data for **3** and the calculated data for **1**-4*R** and **1**-4*S**.

m/*z* 347.1872) and NMR data, indicating seven degrees of unsaturation. The 1D NMR data demonstrated significant similarity to those of **4**, with primary differences observed in the cyclopropane region (C-13: δ_C 18.4 in **4** and 47.8 in **13**; C-14: δ_C 26.3 in **4** and 81.1 in **13**; C-15: δ_C 28.9 in **4** and 82.2 in **13**; C-16: δ_C 73.8 in **4** and 78.9 in **13**; and C-17: δ_C 11.4 in **4** and 20.9 in **13**), suggesting that **13** contained a tetrahydrofuran moiety. This structure was confirmed by HMBC from H-16a (δ_H 3.89) to C-14 (δ_C 81.1), from H-14 (δ_H 4.59) to C-9 (δ_C 45.0)/C-12 (δ_C 32.5), and from H-7 (δ_H 6.06) to C-14 (δ_C 81.1). The NOESY spectrum (Fig. 3) revealed key correlations of H_3-18 with H-14/H-13/H-12a/H_3-20, and H_3-17 with H-13/H-12a, indicating *α*-orientation of these protons. Additionally, NOESY correlations of H-9 with H-11/H-4 indicated *β*-orientation of these protons (Fig. 3). Furthermore, ^{13}C NMR calculations for **13**-4*R** and **13**-4*S** were conducted, and DP4+ probability analysis (Fig. S7) indicated 4*S** as the correct configuration for compound **13**. The absolute configuration of **13** was established as 4*S*, 6*S*, 8*R*, 9*R*,10*R*, 11*R*, 13*R*, 14*R*, 15*R* through comparison of computational and experimental ECD (Fig. S3). Consequently, compound **13** was designated as wallaphnane B.

Previous phytochemical studies demonstrated anti-oxidant properties in tiglianes and rhamnofolanes [6, 12]. Accordingly, compounds **1**-**15** were assessed for their *in vitro* protective effects against H_2O_2-induced cell death in BV-2 cells, utilizing *N*-acetyl-L-cysteine (NAC) as the positive control. As illustrated in Fig. 7, H_2O_2 treatment (0.7 mmol·L^{-1} for 24 h) reduced BV-2 cell viability to approximately 60%, while treatment with compounds **9** and **11** at 20 μmol·L^{-1} restored cell viability

Next, potential targets of active compound **9** were identified using the PharmMapper website, yielding 157 targets [15]. The GeneCards database was utilized to screen anti-oxidant-related targets, resulting in 4281 potential targets. Through intersection analysis, 121 potential common targets were identified. Among these common targets, HMGCR, GSTP1, and SHBG proteins demonstrated higher fit values (> 3.5). Subsequently, the binding interactions of bioactive compound **9** with HMGCR, GSTP1, and SHBG were examined. Molecular docking studies indicated that **9** exhibited strong interactions with these proteins. The logarithms of free binding energies were −7.9, −8.4, and −7.4 kcal·mol^{-1}, respectively. The 9-OH and 20-OH groups formed hydrogen bonds with amino acid residues ILE-762 and GLN-814 of the HMGCR protein, respectively. Compound **9** formed three hydrogen bonds with TYR-7 (9-OH) and LEU-52 (20-OH) of the GSTP1 protein. Additionally, hydrogen bonds between **9** and four amino acid residues (THR-38 and THR-40 with 9-OH; MET-107 and GLY-109 with 20-OH) contributed to its binding with SHBG (Fig. 8). These

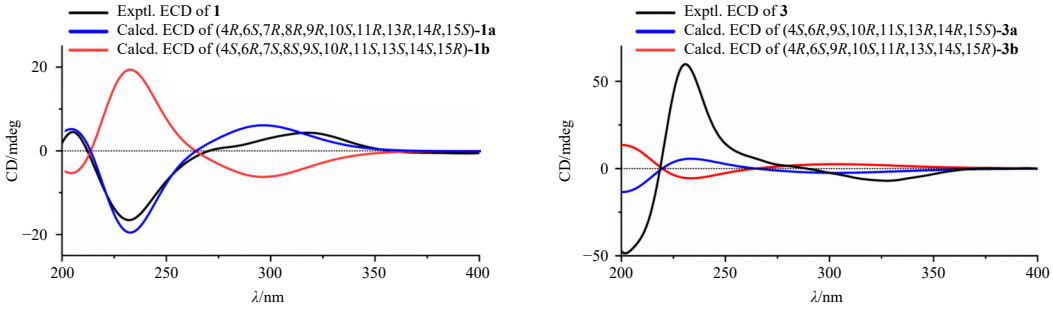

Fig. 5 Experimental and calculated ECD spectra of **1** (left) and **3** (right) in MeOH.

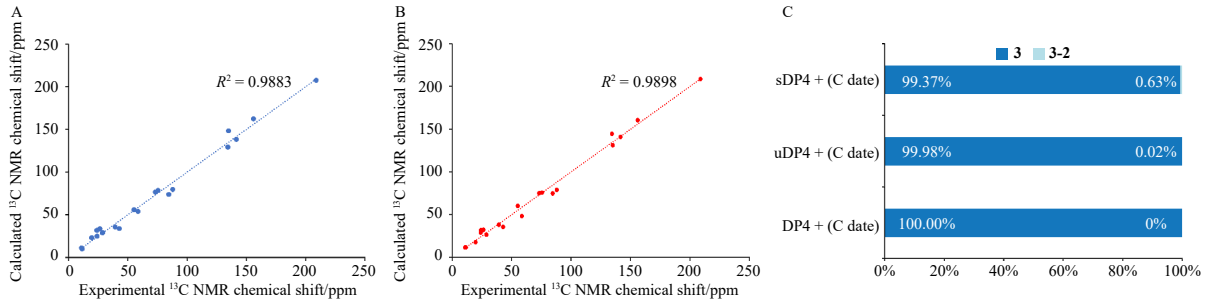

Fig. 6 Linear correlation between the experimental ^{13}C NMR data for **3** and the calculated data for **3** (A) and **3-2** (B), respectively. (C) DP4+ analysis between the ^{13}C NMR data for **3** and the calculated data for **3** and **3-2**.

findings suggest that compound **9** may interact with these proteins to exhibit anti-oxidant effects.

3. Conclusions

The phytochemical investigation of *E. wallichii* resulted in the isolation of 15 compounds, including thirteen previously unreported diterpenoids (**1**–**13**) from the whole plants of *E. wallichii* . The structures were elucidated through extensive 1D and 2D NMR spectroscopic data analysis, and ECD calculations determined the absolute configuration. Wallaphnanes A and B (**12** and **13**) represent daphnane-type diterpenoids, marking the first reported occurrence of this type in these species. In anti-oxidant assays, compounds **9** and **11** demonstrated protective effects on BV-2 cells. Molecular docking studies revealed that bioactive diterpenoid **9** could bind with anti-oxidant targets HMGCR, GSTP1, and SHBG, indicating potential anti-oxidant effects through these interactions.

4. Experimental

4.1. General experimental procedures

Optical rotations and ultraviolet (UV) spectra were measured in CH_3OH using a PerkinElmer 241 polarimeter and a Shimadzu UV 2201 spectrophotometer, respectively. A Bio-Logic MOS-450 instrument was employed for ECD data determination. HR-ESI-MS data were recorded using a Thermo Scientific™ Q Exactive Orbitrap mass spectrometer. 1D and 2D NMR data were acquired on a Bruker AV-600 instrument. Column chromatography (CC) fractionations utilized silica gel (100–200 mesh and 300–400 mesh, Qingdao Marine Chemical Inc.), reversed-phase C_{18} (RP-C_{18}) silica gel (50 μm, YMC, Japan), and MCI gel 20P (75–150 μm, Mitsubishi Chemical Industries, Japan). Preparative high performance liquid chromatography (HPLC) was performed on a LC-6AD liquid chromatography system with a Shimadzu SPD-20A detector using a YMC reversed-phase column (C_{18}, 250 mm × 20 mm, 5 μm).

4.2. Plant material

The whole plants of *E. wallichii* Hook. f. (Euphorbiaceae) were collected from Yunnan Province, China, and authenticated by Prof. Jingming Jia. A specimen (No. 20180801) was deposited at the Key Laboratory of Structure-Based Drug Design & Discovery of Ministry of Education, Shenyang Pharmaceutical University, PR China.

4.3. Extraction and isolation

The initial extraction process of the whole plants of *E. wallichii* (10.8 kg) and fractionation of the extract was previously described [16]. E4 (85.4 g) underwent separation into seven fractions (E41-E47) using MCI-gel CC (CH_3OH/H_2O, 70∶30→0∶100, *V*/*V*). E41 was processed through silica gel CC (petroleum ether–acetone, 100∶0→0∶100, *V*/*V*) to obtain E414. E414 was fractionated using silica gel (petroleum ether–acetone, 80∶1→0∶100, *V*/*V*) to obtain E4143, which was then separated by preparative HPLC (CH_3OH/H_2O, 65∶35, *V*/*V*) to yield compounds **2** (3.4 mg, t_R = 26.2 min) and **4** (5.8 mg, t_R = 38.0 min). E5 (48.0 g) underwent separation using RP-C_{18} silica gel chromatography (CH_3OH/H_2O, 10∶90→100∶0, *V*/*V*) to yield E54, E55, and E56. E54 was subjected to silica gel CC (petroleum ether–acetone, 8∶1→0∶1, *V*/*V*) to produce E541 and E545. E541 underwent further purification by preparative HPLC (CH_3OH/H_2O, 55∶45, *V*/*V*) to yield compound **1** (3.0 mg, t_R = 28.0 min). E545 was purified through preparative HPLC (CH_3OH/H_2O, 75∶25, *V*/*V*) to yeild compound **3** (3.7 mg, t_R = 22.0 min). E55 underwent chromatographed using silica gel CC (petroleum ether–acetone, 8∶1→0∶1, *V*/*V*) to produce E555, followed by preparative HPLC (CH_3OH/H_2O, 60∶40, *V*/*V*) to yield compound **8** (10.2 mg, t_R = 65.0 min) and E5552. E5552 was purified using preparative HPLC (CH_3CN/H_2O, 50∶50, *V*/*V*) to yield compound **13** (2.2 mg, t_R = 28.0 min). E56 underwent separation through silica gel CC (petroleum ether–acetone, 8∶1→0∶1, *V*/*V*) to yield E562, followed by preparative HPLC (CH_3OH/H_2O, 60∶40, *V*/*V*) to yield compound **9** (30.8 mg, t_R = 33.0 min). E6 (58.7 g) was processed using RP-C_{18} silica gel chromatography (CH_3OH/H_2O, 10∶90→90∶10, *V*/*V*) to yield E63 and E65. E63 un-

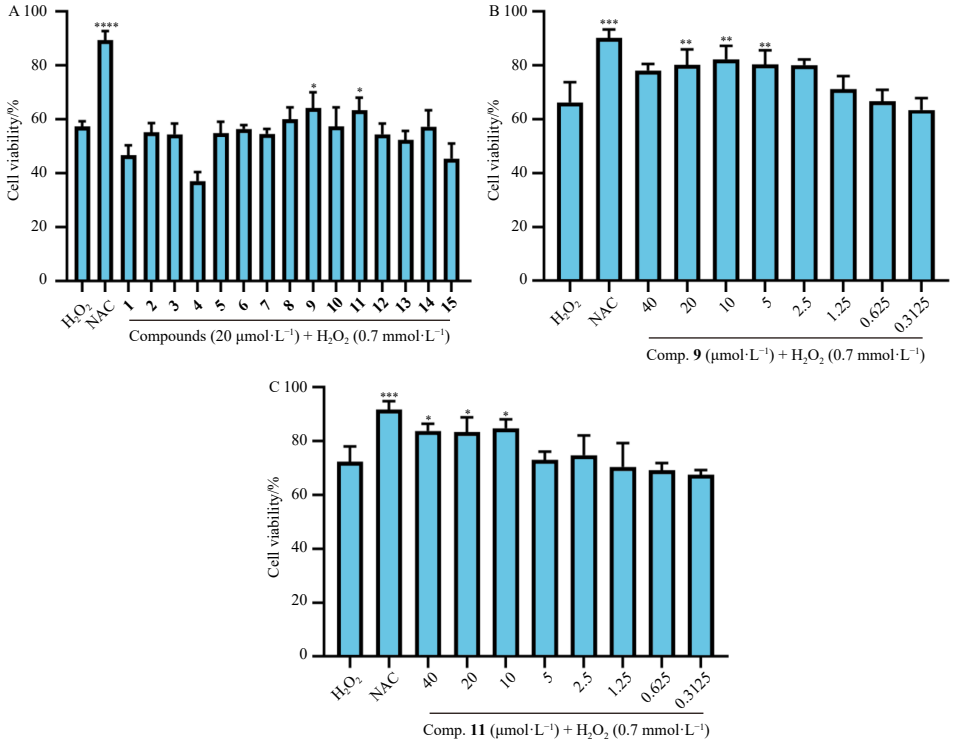

Fig. 7 Effect of compounds **1**–**15** on H_2O_2-induced cell injury in BV-2 cells by the CCK8 assay. Data are mean ± standard error (n = 3) for three independent experiments. $^{****}P < 0.0001$, $^{***}P < 0.001$, $^{**}P < 0.01$, and $^{*}P < 0.05$ *vs* H_2O_2-stimulated group.

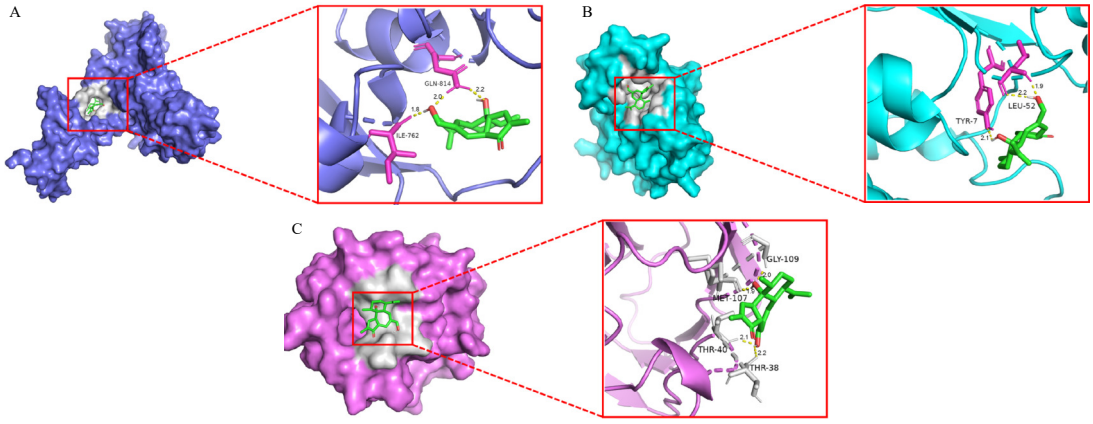

Fig. 8 Molecular docking results of **9** with HMGCR (A), GSTP1 (B), and SHBG (C) proteins. Molecular docking simulations were obtained at the lowest energy conformation, highlighting potential hydrogen contacts of **9**, respectively. Hydrogen bonding interactions are shown by dashes.

derwent separation through silica gel CC (petroleum ether–acetone, 20∶1→0∶1, *V*/*V*) to yield E634, followed by preparative HPLC (CH_3OH/H_2O, 60∶40, *V*/*V*) to yield compound **12** (5.2 mg, t_R = 21.0 min). E65 was separated using silica gel CC (petroleum ether–acetone, 8∶1→0∶1, *V*/*V*) to yield E658, followed by preparative HPLC (CH_3OH/H_2O, 60∶40, *V*/*V*) to yield compound **7** (2.1 mg, t_R = 54.4 min). E7 (64.0 g) underwent chromatography using RP-C_{18} silica gel chromatography (CH_3OH/H_2O, 5∶95→100∶0, *V*/*V*) to yield E74. E74 was separated through silica gel CC (petroleum ether–acetone, 7∶1→0∶1, *V*/*V*) to produce E746 and E748. E746 and E748 underwent chromatography using RP-C_{18} silica gel chromatography (CH_3OH/H_2O, 5∶95→60∶40, *V*/*V*) to yield E7461, E7462, E7463, and E7483, respectively. E7461 was separated by preparative HPLC (CH_3OH/H_2O, 60∶40, *V*/*V*) to obtain compound **11** (4.3 mg, t_R = 16.0 min). E7462 underwent purification using preparative HPLC (CH_3OH/H_2O, 60∶40, *V*/*V*) to obtain compounds **5** (6.3 mg, t_R = 30.0 min) and **6** (3.5 mg, t_R = 28.0 min). Compound **10** (10.3 mg, t_R = 37.0 min) was isolated by preparative HPLC (CH_3OH/H_2O, 60∶40, *V*/*V*) from E7463. E7483 underwent purification through preparative HPLC (CH_3OH/H_2O, 60∶40, *V*/*V*) to give compounds **14** (17.3 mg, t_R = 24.0 min) and **15** (6.4 mg, t_R = 41.0 min).

*4.3.1. Wallichiane G (**1**)*

White amorphous powder; $[\alpha]_D^{20}$ −9.1 (*c* 0.28, CH_3OH); UV (CH_3OH) λ_{max} (log ε) 201.0 (2.21), 220.0 (2.00) nm; The ^{1}H NMR (600 MHz, $CDCl_3$) and ^{13}C NMR (150 MHz, $CDCl_3$) spectroscopic data, see Tables 1 and 3, HR-ESI-MS *m*/*z* 349.2002 $[M + H]^+$ (Calcd. for $C_{20}H_{29}O_5$, 349.2015).

*4.3.2. Wallichiane H (**2**)*

White amorphous powder; $[\alpha]_D^{20}$ −20.2 (*c* 0.50, CH_3OH); UV (CH_3OH) λ_{max} (log ε) 227.8 (4.50) nm; The ^{1}H NMR (600 MHz, $CDCl_3$) and ^{13}C NMR (150 MHz, $CDCl_3$) spectroscopic data, see Tables 1 and 3, HR-ESI-MS *m*/*z* 337.1768 $[M + Na]^+$ (Calcd. for $C_{20}H_{26}O_3Na$, 337.1780).

*4.3.3. Wallicliane I (**3**)*

White amorphous powder; $[\alpha]_D^{20}$ −116.7 (*c* 0.14, CH_3OH); UV (CH_3OH) λ_{max} (log ε) 201.0 (2.31), 215.0 (2.04) nm; The ^1H NMR (600 MHz, $CDCl_3$) and ^{13}C NMR (150 MHz, $CDCl_3$) spectroscopic data, see Tables 1 and 3, HR-ESI-MS *m/z* 393.1889 [M + HCOOH − H]$^-$ (Calcd. for $C_{21}H_{29}O_7$, 393.1913).

*4.3.4. Wallicliane J (**4**)*

White amorphous powder; $[\alpha]_D^{20}$ −31.5 (*c* 0.40, CH_3OH); UV (CH_3OH) λ_{max} (log ε) 202.0 (1.88), 217.0 (1.82) nm; The ^1H NMR (600 MHz, $CDCl_3$) and ^{13}C NMR (150 MHz, $CDCl_3$) spectroscopic data, see Tables 1 and 3, HR-ESI-MS *m/z* 331.1920 [M − H]$^-$ (Calcd. for $C_{20}H_{27}O_4$, 331.1909).

*4.3.5. Wallicliane K (**5**)*

Colorless oils; $[\alpha]_D^{20}$ −114.7 (*c* 0.36, CH_3OH); UV (CH_3OH) λ_{max} (log ε) 202.0 (2.43) nm; The ^1H NMR (600 MHz, CD_3OD) and ^{13}C NMR (150 MHz, CD_3OD) spectroscopic data, see Tables 1 and 3, HR-ESI-MS *m/z* 365.1968 [M − H]$^-$ (Calcd. for $C_{20}H_{29}O_6$, 365.1964).

*4.3.6. Wallicliane L (**6**)*

Colorless oils; $[\alpha]_D^{20}$ −111.3 (*c* 0.28, CH_3OH); UV (CH_3OH) λ_{max} (log ε) 202.0 (2.34) nm; The ^1H NMR (600 MHz, CD_3OD) and ^{13}C NMR (150 MHz, CD_3OD) spectroscopic data, see Tables 1 and 3, HR-ESI-MS *m/z* 365.1968 [M − H]$^-$ (Calcd. for $C_{20}H_{29}O_6$, 365.1964).

*4.3.7. Wallicliane M (**7**)*

Colorless oils; $[\alpha]_D^{20}$ −166.2 (*c* 0.14, CH_3OH); UV (CH_3OH) λ_{max} (log ε) 202.0 (2.37) nm; The ^1H NMR (600 MHz, $CDCl_3$) and ^{13}C NMR (150 MHz, $CDCl_3$) spectroscopic data, see Tables 1 and 3, HR-ESI-MS *m/z* 347.1872 [M − H]$^-$ (Calcd. for $C_{20}H_{27}O_5$, 347.1858).

4.3.8. Wallinofolane A (8)

Yellow oils; $[\alpha]_D^{20}$ −118.1 (*c* 0.42, CH_3OH); UV (CH_3OH) λ_{max} (log ε) 226.0 (2.13) nm; The ^1H NMR (600 MHz, $CDCl_3$) and ^{13}C NMR (150 MHz, $CDCl_3$) spectroscopic data, see Tables 2 and 3, HR-ESI-MS *m/z* 361.1995 [M + HCOOH − H]$^-$ (Calcd. for $C_{21}H_{29}O_5$, 361.2015).

*4.3.9. Wallinofolane B (**9**)*

Yellow oils; $[\alpha]_D^{20}$ +32.8 (*c* 0.40, CH_3OH); UV (CH_3OH) λ_{max} (log ε) 240.0 (2.17) nm; The ^1H NMR (600 MHz, $CDCl_3$) and ^{13}C NMR (150 MHz, $CDCl_3$) spectroscopic data, see Tables 2 and 3, HR-ESI-MS *m/z* 361.1995 [M + HCOOH − H]$^-$ (Calcd. for $C_{21}H_{29}O_5$, 361.2015).

*4.3.10. Wallinofolane C (**10**)*

Colorless oils; $[\alpha]_D^{20}$ +13.4 (*c* 0.68, CH_3OH); UV (CH_3OH) λ_{max} (log ε) 203.0 (2.27) nm; The ^1H NMR (600 MHz, $CDCl_3$) and ^{13}C NMR (150 MHz, $CDCl_3$) spectroscopic data, see Tables 2 and 3, HR-ESI-MS *m/z* 379.2143 [M + HCOOH − H]$^-$ (Calcd. for $C_{21}H_{31}O_6$, 379.2121).

*4.3.11. Wallinofolane D (**11**)*

Colorless oils; $[\alpha]_D^{20}$ +28.4 (*c* 0.42, CH_3OH); The ^1H NMR (600 MHz, CD_3OD) and ^{13}C NMR (150 MHz, CD_3OD) spectroscopic data, see Tables 2 and 3, HR-ESI-MS *m/z* 541.2660 [M + HCOOH − H]$^-$ (Calcd. for $C_{27}H_{41}O_{11}$, 541.2649).

*4.3.12. Wallaphnane A (**12**)*

Colorless oils; $[\alpha]_D^{20}$ −136.6 (*c* 0.22, CH_3OH); UV (CH_3OH) λ_{max} (log ε) 202.0 (2.17), 232 (2.11) nm; The ^1H NMR (600 MHz, $CDCl_3$) and ^{13}C NMR (150 MHz, $CDCl_3$) spectroscopic data, see Tables 2 and 3, HR-ESI-MS *m/z* 335.2216 [M + H]$^+$ (Calcd. for $C_{20}H_{31}O_4$, 335.2217).

*4.3.13. Wallaphnane B (**13**)*

Colorless oils; $[\alpha]_D^{20}$ −123.1 (*c* 0.38, CH_3OH); UV (CH_3OH) λ_{max} (log ε) 201.0 (2.28) nm; The ^1H NMR (600 MHz, $CDCl_3$) and ^{13}C NMR (150 MHz, $CDCl_3$) spectroscopic data, see Tables 2 and 3, HR-ESI-MS *m/z* 347.1872 [M − H]$^-$ (Calcd. for $C_{20}H_{27}O_5$, 347.1858).

*4.4. Acid hydrolysis of **11** and determination of the absolute configuration of sugar*

The experiment was conducted following the previously established method [12]. Detailed experimental procedures are available in the Supporting Information.

4.5. ECD calculations

The theoretical calculations were performed using Gaussian 09. The conformers were optimized using the B3LYP functional and the 6-31G (d) basis set. The optimized conformations underwent ECD calculations using TDDFT at B3LYP/6-311G (d, p) level in MeOH with PCM model. The calculated ECD curve was generated using Multiwfn software [17].

4.6. NMR calculations

Conformational searches were executed using the Spartan 16 program (Wavenfunction, Irvine, CA, USA, 2016) utilizing the MMFF94 force field. The resulting conformers underwent optimization using DFT at the B3LYP/6-31G(d,p) level in the gas phase. The optimized conformations, whose Boltzmann distributions of Gibbs free energies exceeded 0.1%, were utilized for NMR calculations using the GIAO method at the mPW1PW91/6-31G(d,p) level. All calculations incorporated DFT-D4 empirical dispersion correction [18].

4.7. Biological activity

The anti-oxidant assay was conducted according to previous reports [13] and is detailed in the Supplementary data.

4.8. Molecular docking studies

The targets of compound **9** were identified from the PharmMapper (http://www.lilab-ecust.cn/pharmmapper/) website. The anti-oxidant-related targets were retrieved from the GeneCards database (https://www.genecards.org/). The 3D crystal structures of HMGCR (PDB: 2r4f), GSTP1 (PDB: 5j41), and SHBG (PDB: 6pya) were obtained from the RCSB Protein Data Bank. Molecular docking simulations were executed using the software AutoDock Vina in conjunction with AutoDock Tools (ADT 1.5.6).

Funding

This work was supported by the National Natural Science Foundation of China (Nos. 82405016 and 82141216), the Project of Frontier Technology Platform for Research Projects of Liaoning Provincial Department of Education in 2024 (No. LJ232410163056), "Select the best candidates to lead key research projects" of Fujian University of Traditional Chinese Medicine (Nos. XJB2022008 and XJB2023001), the Foundation of Fujian University of Traditional Chinese Medicine (Nos. X2023001-Talent and X2024002-Talent), the Young and Middle-aged Teacher Education Research Project in Fujian Province (No. JZ230023), and the Central Government Guides Local Science and Technology Development Fund Projects (No. 2023L3014).

Supplementary data

Supplementary data for this paper is available upon emailrequest to the corresponding authors.

Declaration of competing interest

The authors declare that they have no known competingfinancial interests or personal relationships that could haveappeared to influence the work reported in this paper.

References

1 Vasas A, Hohmann J. *Euphorbia* diterpenes: isolation, structure, biological activity, and synthesis (2008–2012). *Chem Rev*, 2014, 114: 8579-8612. https://doi.org/10.1021/cr400541j.

2 Zhan ZJ, Li S, Chu W, et al. *Euphorbia* diterpenoids: isolation, structure, bioactivity, biosynthesis, and synthesis (2013–2021). *Nat Prod Rep*, 2022, 39: 2132–2174. https://doi.org/10.1039/D2NP00047D.

3 Du KC, Yang XY, Li JH, et al. Antiproliferative diterpenoids and acetophenone glycoside from the roots of *Euphorbia fischeriana*. *Phytochemistry*, 2020, 177: 112437. https://doi.org/10.1016/j.phytochem.2020.112437.

4 Pan LL, Fang PL, Zhang XJ, et al. Tigliane-type diterpenoid glycosides from *Euphorbia fischeriana*. *J Nat Prod*, 2011, 74: 1508-1512. https://doi.org/10.1021/np200058c.

5 Wei YL, Yu ZL, Huo XK, et al. Diterpenoids from the roots of *Euphorbia fischeriana* and their inhibitory effects on α-glucosidase. *J Asian Nat Prod Res*, 2018, 20:977-984. https://doi.org/10.1080/10286020.2017.1367923.

6 Yuan FY, Tang ZY, Huang D, et al. Tigliane and rhamnofolane glycosides from *Euphorbia wallichii* prevent oxidative stress-induced neuronal death in PC-12 cells. *Bioorg Chem*, 2022, 128: 106103. https://doi.org/10.1016/j.bioorg.2022.106103.

7 Li H, Wei WY, Xu HX. Drug discovery is an eternal challenge for the biomedical sciences. *Acta Mater Med*, 2022, 1: 1-3. https://doi.org/10.15212/AMM-2022-1001.

8 Pan L, Zhou P, Zhang X, et al. Skeleton-rearranged pentacyclic diterpenoids possessing a cyclobutane ring from *Euphorbia wallichii*. *Org Lett*, 2006, 8: 2775-2778. https://doi.org/10.1021/ol0608552.

9 Li H, Yang P, Zhang EH, et al. Antimicrobial ent-abietane-type diterpenoids from the roots of *Euphorbia wallichii*. *J Asian Nat Prod Res*, 2021, 23: 652-659. https://doi.org/10.1080/10286020.2020.1758931.

10 Wan LS, Nian Y, Peng XR, et al. Pepluanols C–D, two diterpenoids with two skeletons from *Euphorbia peplus* . *Org Lett*, 2018, 20: 3074-3078. https://doi.org/10.1021/acs.orglett.8b01114.

11 Yang DS, Peng WB, Yang YP, et al. Chemical constituents from *Euphorbia wallichii* and their biological activities. *J Asian Nat Prod Res*, 2015, 17: 946-951. https://doi.org/10.1080/10286020.2015.1038525.

12 Wang YL, Zhu M, Liang J, et al. Diterpenoids from the whole plant of *Euphorbia wallichii* and their protective effects on H_2O_2-induced BV-2 microglial cells injury. *Bioorg Chem*, 2022, 128: 106067. https://doi.org/10.1016/j.bioorg.2022.106067.

13 Wang YL, Wang H, Leng YX, et al. Structurally intriguing diterpenoids from *Euphorbia wallichii* Hook. f. with potential antioxidant activity. *Phytochemistry*, 2024, 221: 114043. https://doi.org/10.1016/j.phytochem.2024.

14 Dou WT, Hao YP, Liu JL, et al. Two novel phorbol esters from *Croton tiglium* L. *J Chin Pharm Sci*, 2016, 25: 771-778. https://doi.org/10.5246/jcps.2016.10.086.

15 Wang X, Shen YH, Wang SW, et al. PharmMapper 2017 update: a web server for potential drug target identification with a comprehensive target pharmacophore database. *Nucleic Acids Res*, 2017, 45: 356-360. https://doi.org/10.1093/nar/gkx374.

16 Wang YL, Jiang QH, Sun DJ, et al. *Ent*-kauranes and *ent*-atisanes from *Euphorbia wallichii* and their anti-inflammatory activity. *Phytochemistry*, 2023, 210: 113643. https://doi.org/10.1016/j.phytochem.2023.113643.

17 Lu T, Chen FW. Multiwfn: a multifunctional wavefunction analyzer. *J Comput Chem*, 2012, 33: 580-592. https://doi.org/10.1002/jcc.22885.

18 Smith SG, Goodman JM. Assigning stereochemistry to single diastereoisomers by GIAO NMR calculation: the DP4 probability. *J Am Chem Soc*, 2010, 132: 12946-12959. https://doi.org/10.1021/ja105035r.